Technical University of Denmark

DTU

Self-pulsation threshold of Raman amplified Brillouin fiber cavities

Ott, Johan Raunkjær; Pedersen, Martin Erland Vestergaard; Rottwitt, Karsten

DTU Library
Technical Information Center of Denmark

Self-Pulsation threshold of Raman amplified Brillouin fiber cavities

J. R. Ott, M. E. V. Pedersen, and K. Rottwitt

Technical University of Denmark (DTU),Department of Photonics Engineering (DTU Fotonik), Build. 343, DK-2800, Kgs. Lyngby, Denmark.

jrot@fotonik.dtu.dk

Abstract: An implicit equation for the oscillation threshold of stimulated Brillouin scattering from Raman amplified signals in fibers with external feedback is derived under the assumption of no depletion. This is compared to numerical investigations of Raman amplification schemes showing good agreement for high reflectivities. For low reflectivities and high attenuation or long fibers, the assumption of no depletion is shown not to be valid. In these cases the effects of the depletion on the self-pulsation is examined.

© 2009 Optical Society of America

OCIS codes: (060.4370) Nonlinear optics, fibers, (060.2320) Fiber optics amplifiers and oscillators, and (290.5900) Scattering, stimulated Brillouin .

References and links

[1] G. P. Agrawal, *Nonlinear Fiber Optics*, Third Edition, (Academic Press, San Diego, 2001).

[2] E. P. Ippen, "Low-power quasi-cw Raman oscillator," Appl. Phys. Lett. **16**, 303-305 (1970).

[3] R. V. Johnson and J. H. Marburger, "Relaxation oscillation in stimulated Raman and Brillouin scattering," Phys. Rev. A **4**, 1175-1182 (1971).

[4] E. P. Ippen and R. H. Stolen, "Stimulated Brillouin scattering in optical fibers," Appl. Phys. Lett. **21**, 539-541 (1972).

[5] R. G. Smith, "Optical Power Handling Capacity of Low Loss Optical Fibers as Deterined by Stimulated Raman and Brillouin Scattering," App. Opt. **11**, 2489-2494 (1972).

[6] D. Cotter, "Stimulated Brillouin scattering in monomode optical fibers," Opt. Commun. **4**, 10-19 (1983).

[7] I. Bar-Joseph, A. A. Friesem, E. Lichtman, and R. G. Waarts, "Steady and relaxation oscillations of stimulated Brillouin scattering in single-mode optical fibers," J. Opt. Soc. Am. B. **2**, 1606 (1985).

[8] A. L. Gaeta and R. W. Boyd, "Stimulated Brillouin scattering in the presence of external feedback," J. Nonlinear Opt. Phys. Mater. **1**, 581-594 (1992).

[9] M. Dämmig, G.Zinner, F. Mitschke, and H. Welling, "Stimulated Brillouin scattering in fibers with and without external feedback," Phys. Rev. A **48**, 3301-3309 (1993).

[10] J. H. Lee, T. Tanemura, and K. Kikuchi, "Experimental comparison of a Kerr Nonlinearity figure of merit including the stimulated Brillouin scattering threshold for state-of-the-art nonlinear optical fibers," Opt. Letters **30**, 1968-1970 (2005).

[11] V. I. Kovalev and R. G. Harrison, "Continuous wave stimulated Brillouin scattering in optical fibers: New results and applications for high power lasers," in *Topical Problems of Nonlinear Wave Physics*, Proc. SPIE **5975**, 59750L-1-13 (2006).

[12] J. W. Lou, F. K. Fatemi, and M. Currie, "Brillouin fibre laser enhanced by Raman amplification," Elect. Lett. **40**, 1044-1046 (2004).

[13] G. Ravet, A.A. Fotiadi, M. Blondel, and P. Mégret, "Passive Q-switching in all-fibre Raman laser with distributed Rayleigh feedback," Elect. Lett. **40**, 528-529 (2004).

[14] A. A. Fotiadi, P. Mégret, and M. Blondel, "Dynamics of a self-Q-switched fiber laser with a Rayleigh–stimulated Brillouin scattering ring mirror," Opt. Lett. **29**, 1078-1080 (2004).

[15] A. N. Pilipetskii and V. V. Shkunov, "Calculation of the threshold and of the efficiency of conversion by stimulated scattering in an amplifying medium," Sov. J. Quantum Elect. **15**, 284-286 (1985).

[16] M. E. V. Pedersen, J. R. Ott, and K. Rottwitt, "Self-Pulsation in Raman Fiber Amplifiers," presented at the Eleventh International Conference on Transparent Optical Networks, Island of São Miguel, Azores, Portugal, 28 June-2 July 2009.

[17] K. Rottwitt and A. J. Stentz, "Raman Amplification in Lightwave Communication Systems," in *Optical Fiber Telecommunications*, Chap. 5, (Academic Press, San Diego, Calif., 2002).

1. Introduction

When light interacts with a medium, acoustic waves are generated on which the light is reflected. This reflected optical wave, in the following referred to as the Brillouin wave, will have a frequency in the order of 10 GHz lower than the incident light for silica based fibers [1]. This phenomenon, known as stimulated Brillouin scattering (SBS), is the nonlinear optical phenomenon with the lowest threshold for narrow-band light. This low threshold has been discussed in relation to limitations of continuous wave (CW) high power fiber lasers and has thus been an active research subject since the achievement of low loss optical fibers [2–11]. The current investigation is motivated by the recent use of Raman amplification of a Brillouin fiber laser [12] and experimental observation and theoretical modeling of passive Q-switching in Raman fiber lasers due to Brillouin self-pulsation [13, 14].

When propagating CW light in optical fibers the backward propagating Brillouin wave is amplified due to SBS, where the input CW signal act as a pump. As the power of the input CW signal is increased, the Brillouin gain is increased and consequently the backward propagating power of the Brillouin wave increases to a level where it starts to deplete the input signal. If the input signal power is increased even further, the depletion causes the signal power to drop so that the system eventually enters a mode of self-pulsation. If feedback is introduced to the system ie. through reflections at the fiber ends, the input power threshold of this oscillating behavior is reduced. The threshold condition for SBS and stimulated Raman scattering individually in the absence of feedback was first given by R. G. Smith [5]. In the case of low reflectivity the SBS threshold was given by A. L. Gaeta and R. W. Boyd [8] including the material response time and for arbitrary external feedback by M. Dämmig *et al.* [9] not including the material response time.

In the following a threshold condition for oscillations due to SBS of a Raman amplified signal is derived for arbitrary external feedback under assumptions on the depletion due to the SBS. The derivation follow the method used by R. G. Smith [5] and M. Dämmig *et al.* [9]. The analytic results are compared to numerical investigations of a discrete and a distributed Raman amplification schemes. From these specific examples the result of depletion on the threshold condition is shown, a point which to the knowledge of the authors has not been addressed previously.

2. Theory

The present work focus on the effects of loss and Raman amplification and in the following an analytical equation for the power threshold, at which self-pulsation occur, is derived. The setup considered here, shown in Fig. 1, consist of a single mode, inversion symmetric fiber of length L placed between two reflectors having power reflectivities, R^+ in the signal input end and R^- in the signal output end; both reflects the light back into the fiber and thus creates a Fabry-Pérot cavity. The cavity can thus arrive either on purpose or unintentionally i.e. due to fiber splices. It is noted that the length between the two reflectors considered here is in the order of hundreds of meters to kilometers. Consequently the longitudinal modespacing is small ($\sim$500 kHz for a 200 m cavity) compared to the linewidth of the Brillouin gain spectrum (in the order of 20-100 MHz for silica based fibers [1]). Thus the investigation does not involve mode locking due to cavity resonances, but Brillouin self-pulsation due to wave dynamics. For a polarization maintaining single mode fiber, neglecting four wave mixing e.g. due to phase mismatch, neglecting higher order Brillouin scattering, and assuming instantaneous material

response the governing equations can be expressed in power as [1]

$$\frac{1}{v_{g,R}}\frac{\partial P_R^{\pm}}{\partial t} \pm \frac{\partial P_R^{\pm}}{\partial z} = -g_R\frac{\omega_R}{\omega_S}P_R^{\pm}(P_S^+ + P_S^- + P_B^+ + P_B^-) - \alpha_R P_R^{\pm},$$ (1a)

$$\frac{1}{v_{g,S}}\frac{\partial P_S^{\pm}}{\partial t} \pm \frac{\partial P_S^{\pm}}{\partial z} = -g_B\frac{\omega_B}{\omega_S}P_S^{\pm}P_B^{\mp} + g_R P_S^{\pm}(P_R^+ + P_R^-) - \alpha_S P_S^{\pm},$$ (1b)

$$\frac{1}{v_{g,B}}\frac{\partial P_B^{\pm}}{\partial t} \pm \frac{\partial P_B^{\pm}}{\partial z} = g_B P_S^{\mp}P_B^{\pm} + g_R P_B^{\pm}(P_R^+ + P_R^-) - \alpha_B P_B^{\pm},$$ (1c)

where $P_S^{\pm} = P_S^{\pm}(z,t)$, $P_B^{\pm} = P_B^{\pm}(z,t)$ and $P_R^{\pm} = P_R^{\pm}(z,t)$ are the powers of the signal, Brillouin and Raman waves, the +(-) superscripts indicates forward(backward) propagating waves, g_i is the Brillouin ($i = $ B) or Raman ($i = $ R) gain coefficient, z is the length, and t is the time. ω_S, ω_B and ω_R are the angular frequencies of the signal, Brillouin and Raman waves respectively. Their ratio takes into account the difference in energy between the Raman wave, the signal, and Brillouin waves. Since the change in frequency of the acoustic wave is usually very small compared to the optical frequency, the ratio between ω_S and ω_B is approximately 1. Furthermore α_S, α_B, and α_R are the attenuation coefficients and since $\omega_B \approx \omega_S$ then $\alpha_S \approx \alpha_B = \alpha$ is used in the following. $v_{g,S}$, $v_{g,B}$, and $v_{g,R}$ are the group velocities, which can assume arbitrary values in the analytical approach. The pump for the Raman amplifier is assumed to have a line width broad enough to disregard Brillouin contributions. The assumption of an instantaneous material response is valid for long temporal pulses compared to the response of the material as in the present case.

The boundary conditions (BC)s for the Fabry-Pérot cavity are

$$P_R^+(0,t) = R_R^+ P_R^-(0,t) + P_R^{in,+}, \qquad\qquad P_R^-(L,t) = R_R^- P_R^+(L,t) + P_R^{in,-},$$ (2a)

$$P_S^+(0,t) = R_S^+ P_S^-(0,t) + P_S^{in,+}, \qquad\qquad P_S^-(L,t) = R_S^- P_S^+(L,t),$$ (2b)

$$P_B^+(0,t) = R_B^+ P_B^-(0,t) + \varepsilon^+, \qquad\qquad P_B^-(L,t) = R_B^- P_B^+(L,t) + \varepsilon^-,$$ (2c)

where $P_i^{in,\pm}$ is the signal ($i = $ S) or Raman ($i = $ R) input power, $\varepsilon^{\pm}$ is the Brillouin seed due to vacuum or thermal lattice fluctuations and $R_i^{\pm}$ are the cavity end reflectivities for which the superscript $+(-)$ refer to the reflection of the waves in the $-(+)$ into the $+(-)$ direction. The setup is illustrated in Fig. 1.
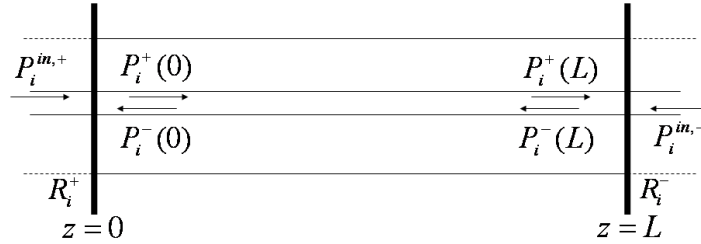

Fig. 1. A fiber cavity of length L with power reflectivity R_i^+ in the left end and R_i^- in the right end creates a cavity. A CW input signal in this produce a Brillouin wave in the opposite direction. Both waves are amplified by a Raman amplifier. The signal output power, given by $P_S^{out}(t) = (1 - R_S^-)P_S^+(L,t)$, oscillates in case of high signal input power levels.

A way of defining the threshold condition, as it is done in Refs. [5] and [9], is when the input signal power at which the intracavity SBS power in the signal input end in steady state reaches

a fraction, r, of the intracavity signal power at the input end, i.e.

$$P_B^-(0) = rP_S^+(0). \tag{3}$$

r signifies the limit at which SBS depletion of the signal is nearly negligible. It will shortly be related to an experimentally obtainable parameter involving the low reflectivity limit of the threshold. The self-pulsations occur when the Brillouin wave depletes the signal. The power threshold, P^{thr}, is then given by the BC's from insertion of $P_S^+(0) = R_+ P_S^-(0) + P_{\text{thr}}$ in Eq. 3. It is noted that the threshold power defined here is the experimentally obtainable input signal power thus different from the steady-state intra cavity signal power at the signal input end, $P_S^+(0)$, used in Ref. [9]. The value $r = 1$ was used by R. G. Smith in Ref. [5] yielding the estimate for no Raman amplification nor external feedback of $I_{\text{thr}} \approx 21\alpha/(g_B A_{\text{eff}})$, with I_{thr} being the threshold intensity and A_{eff} the effective area of the signal.

The threshold is defined as the point immediately before the Brillouin wave significantly influence the signal. This implies that steady state is assumed for all the waves and the signal is assumed not to be effected by the Brillouin scattering. Furthermore the Raman pump is assumed undepleted. This gives, see Appendix A,

$$P_S^+(z) = \tilde{P}_S G^+(z), \tag{4a}$$

$$P_S^-(z) = \tilde{P}_S \rho_S^- G^+(L) G^-(z), \tag{4b}$$

$$P_B^+(z) = \tilde{P}_B^+ G^+(z) \exp\left[g_B \tilde{P}_S \rho_S^- G^+(L) J^+(z)\right], \tag{4c}$$

$$P_B^-(z) = \tilde{P}_B^- G^+(L) G^-(z) \exp\left[g_B \tilde{P}_S J^-(L)\right] \exp\left[-g_B \tilde{P}_S J^-(z)\right], \tag{4d}$$

where $G^\pm$, $\tilde{P}_i^\pm$ and $J^\pm$ have been introduced for convenience and will be defined in the following. The effective Raman gain is defined as

$$G^\pm(z) = \exp\left\{\mp\alpha z \pm \frac{g_R}{\alpha_R}\left[\tilde{P}_R^+\left(1 - e^{-\alpha_R z}\right) + \tilde{P}_R^- e^{-\alpha_R L}\left(e^{\alpha_R z} - 1\right)\right]\right\}, \tag{5}$$

similar to the Raman gain [1] except for the forward and backward Raman input powers being replaced with the effective forward and backward Raman input powers

$$\tilde{P}_R^\pm = \frac{P_R^{\text{in},\pm} + \tilde{R}_R^\pm P_R^{\text{in},\mp}}{1 - \tilde{R}_R^+ \tilde{R}_R^-}, \tag{6}$$

with $\tilde{R}_R^\pm = R_R^\pm \exp(-\alpha_R L)$ the attenuated reflectivies. For long fiber lengths the attenuated reflectivies go to zero and the effective Raman gain equal the Raman gain.

In Eqs. (4) the effective signal and Brillouin input powers are defined as

$$\tilde{P}_S = \frac{P_S^{\text{in}}}{1 - \rho_S^+ \rho_S^-}, \qquad \tilde{P}_B^\pm = \frac{\varepsilon^\pm + \rho_B^\pm \varepsilon^\mp}{1 - \rho_B^+ \rho_B^- \exp\left\{g_B \tilde{P}_S[\rho_S^- J^+(L) - J^-(L)]\right\}}, \tag{7}$$

with the effective reflectivities $\rho_i^\pm = R_i^\pm G^+(L)$. Furthermore the effective position of the forward and backward Brillouin waves are defined as

$$J^+(z) = G^+(L)\int_0^z G^-(z')\mathrm{d}z', \qquad J^-(z) = \int_0^z G^+(z')\mathrm{d}z', \tag{8}$$

where analytical expressions for $J^\pm(z)$ are given in Appendix B. With this definition, $J^+(L)$ and $J^-(L)$ corresponds to the effective Brillouin fiber lengths of the forward and backward

propagating waves respectively. If no Raman gain is introduced these reduce to the conventional effective length

$$J^+(L) = J^-(L) = \frac{1 - \exp(-\alpha L)}{\alpha}. \tag{9}$$

When the Raman gain is introduced $J^+(L)$ differ from $J^-(L)$ since the forward and backward propagating signal in general experience different gain.

With Eqs. (4) the threshold power in the absence of feedback is given, using Eq. (3), as

$$r P_{R=0}^{\text{thr}} = \varepsilon^- G_0^+(L) \exp\left[g_B P_{R=0}^{\text{thr}} J_{R=0}^-(L)\right], \tag{10}$$

where the index $R = 0$ indicates that all the reflectivities are zero.

An implicit equation for the cavity threshold can now be found by taking the ratio between Eqs. (3) and (10) giving

$$\frac{\tilde{P}^{\text{thr}}}{P_{R=0}^{\text{thr}}} = \frac{G^+(L)}{G_{R=0}^+(L)} \frac{\exp\left[-g_B P_{R=0}^{\text{thr}} J_{R=0}^-(L)\right] - \rho_B^- \eta \exp\left\{g_B[\tilde{P}^{\text{thr}} \rho_S^- J^+(L) - P_{R=0}^{\text{thr}} J_{R=0}^-(L)]\right\}}{\exp\left[-g_B \tilde{P}^{\text{thr}} J^-(L)\right] - \rho_B^+ \rho_B^- \exp\left[g_B \tilde{P}^{\text{thr}} \rho_S^- J^+(L)\right]}, \tag{11}$$

where the threshold signal input power is

$$\tilde{P}^{\text{thr}} = \frac{P^{\text{thr,in}}}{1 - \rho_S^+ \rho_S^-}, \tag{12}$$

and the ratio between the Brillouin inputs is

$$\eta = \frac{\varepsilon^+}{\varepsilon^-}. \tag{13}$$

Eq. (11) is the SBS oscillation threshold condition for Raman amplified Brillouin fiber cavities. This implicit equation is the main result of this work. The arbitrary parameter r has been replaced by the experimentally obtainable $P_{R=0}^{\text{thr}}$, i.e. the threshold in the absence of external feedback. The result, Eq. (11), reduces to the experimentally verified threshold obtained in Ref. [9] if no Raman gain is included and thus also reduces to the resulting equations of Ref. [8] for equal and high reflectivity in both the fiber ends.

Similar results have been achieved for erbium doped amplifiers without taking the feedback into account, but including the temperature dependence on the Brillouin coefficient [11] [15].

3. Validation

In the following the signal power threshold is calculated using Eq. (11) and compared to numerical results. This investigation begin by using realistic parameters for which the oscillation threshold of a discrete and a distributed backward Raman fiber amplification schemes are found. Then the effects of depletion on the threshold is examined and at last the effect of the different parameters of Eq. (11) are studied. The validation is performed in order to show the applications of the derived threshold condition and point out its limitations. For the investigation the attenuations of all waves are identical, the reflectivities of all waves are identical and the reflections at both fiber ends are equal so that a round-trip reflectivity, $R_i^+ R_i^- = R^2$, is defined.

The numerical investigation was conducted as described in Ref. [16]. In the analytical approach the experimentally obtainable value of r was chosen so as to match the numerical results. As mentioned in the previous section the value of r describes the signal threshold power as the reflectivities go to zero.

For the amplification schemes the input power of the Raman amplifiers has been chosen such that they model an optical communication scheme. First a discrete amplifier case with a gain of 20 dB over a fiber of 200 m, e.g to counterbalance a 20 dB loss in a subsequent 100 km fiber. Secondly a distributed amplifier case with a 20 dB gain counterbalancing a simultaneous 20 dB loss in a 100 km fiber. The Raman input powers used to achieve the mentioned gains are calculated in absence of external feedback [17]. The coefficients of the two different amplifier schemes are shown in Table 1. The coefficients correspond to standard silica based optical fibers with different amounts of germanium dopants. If other fibers are used the assumption of instantaneous material response might not be valid.

	L	g_{B}	g_{R}	α	$P_{\mathrm{R}}^{\mathrm{in},+}$
Discrete Amp.	200 m	0.8 $(\mathrm{Wm})^{-1}$	5 $(\mathrm{Wkm})^{-1}$	0.8 dB/km	4.7 W
Distributed Amp.	100 km	0.14 $(\mathrm{Wm})^{-1}$	0.7 $(\mathrm{Wkm})^{-1}$	0.2 dB/km	0.3 W

Table 1. The used values of the amplifier schemes.

The numerical and analytical results are given in Figs. 2 and 3 where the oscillation power threshold vs. the round trip reflectivity in dB, defined as $10\log_{10}(R^2)$, is shown. The solid line corresponds to the scheme in which Raman amplification is used to counterbalance fiber losses, the dashed line show the threshold without the amplification and the dash-dotted line show the threshold for lossless fibers. The thin lines with errorbars are the numerically obtained results.

When the transmitted signal become unstable, i.e. pulsed, both the Brillouin scattered signal as well as the transmitted input signal exhibit steady state oscillations. If both fiber ends are cleaved at a 90° angle to the direction of the fiber, the reflection at each end equals ≈ -15 dB, corresponding to a round trip reflectivity of -30 dB however, typical components and splices have significant lower reflections.

The power threshold for the discrete amplifier scheme is shown in Fig. 2 versus different round-trip reflectivity. The figure contain three pairs of curves one with a 20 dB gain, one without the gain and one without gain nor loss where a stable output, i.e. not oscillating, occur for input powers to the left of the curves. The thick lines corresponds to the derived threshold while the thin lines with error bars corresponds to numerically found thresholds. The numerical and analytical found thresholds coincide well for high reflectivities, but deviate slightly just before reaching the low reflectivity limit. This deviation is further investigated shortly. The addition of gain is found to reduce the stability region as expected since it increase the signal and Brillouin waves and thus effectively increases the Brillouin gain coefficient. This may also be seen from the derived equation, Eq. (11), as the addition of Raman amplification increase the effective Brillouin fiber length $J^{\pm}(L)$.

By comparing the curves for propagation with and without loss it is seen that the stability region increase as attenuation occur. This feature is more pronounced for the distributed amplifier scheme, Fig. 3, as the fiber is longer and thus more lossy. The increase of the stability region can be understood intuitively as losses will reduce oscillations. This is also seen from Eq. (11) as increasing the loss decrease the effective Brillouin fiber length which might be most easily seen in the case of no amplification where $J^{\pm}(L) = [1 - \exp(-\alpha L)]/\alpha$ which goes to zero as α becomes large.

Another very noticeable feature of Fig. 3 is that the addition of losses increase the difference between the analytical and numerical curves. The difference for low reflectivities is due to the validity of neglecting depletion of the signal and the Raman waves. The depletion reduces the power in the signal and the Raman waves thus reducing the power transfer to the Brillouin wave thereby increasing the needed signal input power for oscillations. For high round-trip reflectivity the cavity reflectivity is higher than the attenuation keeping the powers at a high level
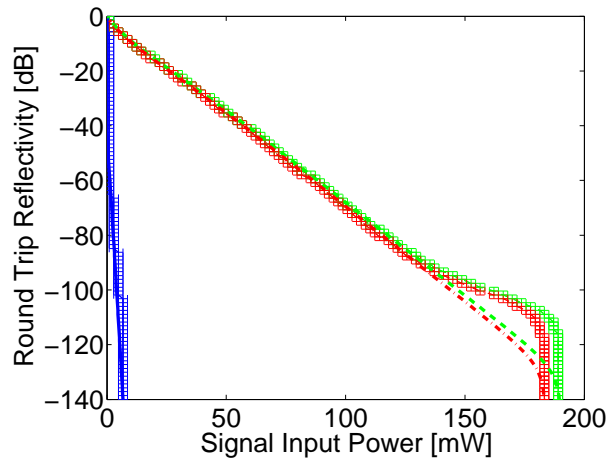
Fig. 2. Oscillation power threshold for the discrete Raman amplifier vs. different round trip reflectivity, defined as $10\log_{10}(R^2)$. The blue solid lines corresponds to the scheme with a Raman gain of 20 dB, the green dashed lines show the threshold without the amplification and the red dash-dotted lines show the threshold for lossless fibers. The thick lines are the derived results and the thin lines with error bars are the numerically obtained results. The regions below the curves corresponds to CW output.
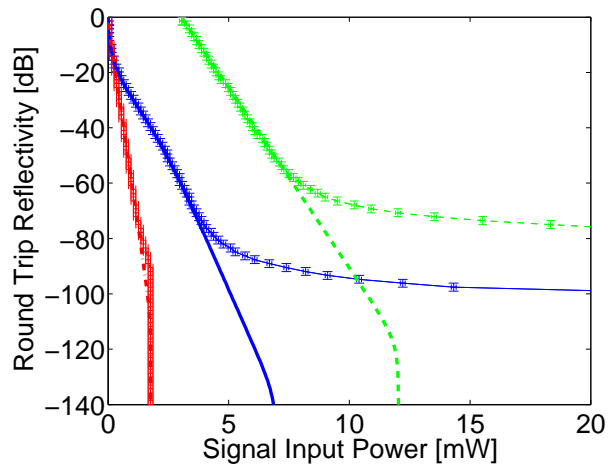

Fig. 3. Oscillation power threshold for the distributed Raman amplifier vs. different round trip reflectivity, defined as $10\log_{10}(R^2)$. The blue solid lines corresponds to the scheme in which Raman amplification is used to counterbalance fiber losses as described in the text, the green dashed lines show the threshold without the amplification and the red dash-dotted lines show the threshold for lossless fibers. The thick lines are the derived results and the thin lines with error bars are the numerically obtained results. The regions below the curves corresponds to CW output.

making depletion negligible. Adding the Raman amplification is seen to increase the region in which the approximation of undepletion is valid as the gain counterbalance the losses. In Fig. 4 the numerical stability calculation of the Raman amplified propagation shown in Fig. 3 is performed for the three cases of i) depletion included, the thin solid, ii) without depletion on the Raman wave, the thin dashed line, and iii) without depletion on the Raman wave nor the signal wave, thin dash dotted line, all with error bars. In addition the derived analytical solution also shown in Fig. 4, is shown as the thick solid line. The thin dash dotted line follow the analytical solution within the numerical resolution as it should. Furthermore, it is seen that the dashed line lie between the line with full depletion and the derived analytical solution indicating that the difference is caused by the validity of the assumption of undepleted signal and Raman pump. The assumption of negligible depletion is thus only valid for short fibers, low losses or high reflectivities. The derived Eq. (11) thus always underestimate the threshold compared to the actual threshold.

The fact that Eq. (3) might seem contradictory to the experimental confirmation of the threshold without amplification, derived in Ref. [9], which Eq. (11) reduce to in the limit of no Raman amplification. The reader should though not worry as the experiment of Ref. [9] was performed on a short fiber of less than 200 m and did not consider reflections below ~ -85 dB.
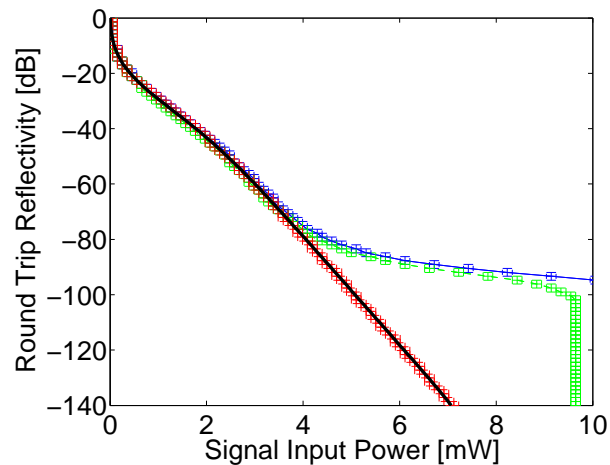

Fig. 4. The threshold for the distributed Raman amplified scheme, shown in Fig. 3, which is numerically calculated in the three cases of i) propagation including depletion, the thin blue solid line, ii) propagation without depletion on the Raman wave, the thin green dashed line, and iii) propagation without depletion on the Raman wave nor the signal wave, thin red dash dotted line, all with error bars. The thick black solid line show the derived threshold.

At last the threshold of the discrete Raman amplifier scheme with parameters in Table 1 is investigated by changing the parameters individually. In Fig. 5 seven different cases are studied. The thick lines show the derived Eq. (11) while the thin marked lines corresponds to the numerical calculations. The blue, green and red colored lines show the threshold for backward, forward and bidirectional Raman amplifier schemes respectively, all with a gain of 10 dB in absence of external feedback. The three schemes yield exactly the same threshold in the analytical model. In the numerical calculations the backward amplification scheme is slightly more stable than the forward amplification scheme and the differences become more pronounced at the low reflectivity limit. This is because the signal wave for the backward amplification schemes in case of no external feedback has lower path average power than the forward amplification scheme and thus decrease the energy transfer to the Brillouin wave compared to the forward

amplification scheme. Simultaneously the lower path average power increase the effects of depletion thereby making the analytical threshold differ slightly more from the numerical results for the backward amplification scheme compared to the forward and bidirectional schemes. The stability of the bidirectional scheme lie between the two others as it is a combination of these. As the feedback increases the backward and forward schemes approach the bidirectional scheme as the reflections in effect cause bidirectional amplification.

The light-blue line show that the threshold for the backward amplification scheme with only 5 dB gain has a higher threshold compared to the blue line with the same scheme, but 10 dB gain. This is expected as decreasing the gain increase the stability and is also apparent from the effective Brillouin cavity length, $J^{\pm}(L)$, which decrease as the Raman input decrease. The opposite case of increasing the gain to 20 dB was shown in Fig. 2 yielding a decrease of the stability region. The yellow and black lines show the threshold for no amplification and including losses and excluding losses respectively. These curves are also shown in Fig. 2. The pink line show the backward amplification scheme with 10 dB gain, but a 1 km cavity. Increasing the cavity length increase the effective Brillouin cavity length and thus decrease the power threshold.

It is be noted that the analytical threshold yield qualitatively if not quantitatively the same results as the numerical calculations. Calculation times are though in the order of seconds for the implicit analytical equation where the numerical calculations take in the order of hours even days.
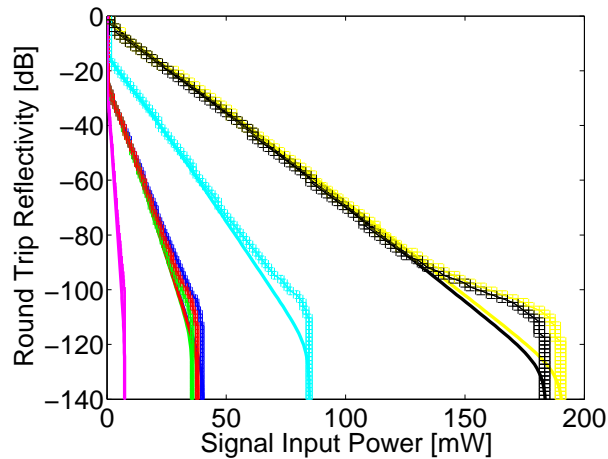

Fig. 5. Comparison of forward, backward and bidirectional amplification and an investigation of the effect of propagation length, loss and amount of amplification. The general values of $L = 200$ m, $g_B = 0.8$ (Wm)$^{-1}$, $g_R = 5$ (Wm)$^{-1}$ and $\alpha = 0.8$ dB/km when not explicitly stated otherwise. The thick lines indicates the analytically found threshold while the thin lines with error bars show the corresponding numerical calculations. Color codes are as follows: Blue: Backward amplification, 10 dB gain. Green: Forward amplification, 10 dB gain. Red: Bidirectional amplification, 10 dB gain. Light-blue: Backward amplification, 5 dB gain. Pink: Backward amplification, 10 dB gain, 1 km cavity. Yellow: No amplification. Black: No amplification nor loss.

4. Conclusion

A power threshold condition, Eq. (11), for SBS induced oscillations of a Raman amplified signal is derived and compared to numerical investigations showing quantitative good agreement

for high reflectivities. The difference in the numerical and analytical model for low reflectivities, occurring for high attenuation or long fibers, is shown to be caused by the depletion of the signal and Raman gain therefore decrease the transfer of power to the Brillouin wave and thus increase the threshold for self-pulsation. The derived threshold condition thus always underestimate the threshold compared to the actual threshold. The analytical threshold show good agreement for short fibers, low losses and high reflectivity as this keep power levels in the cavity high thus making depletion negligible.

Appendix A.

For the determination of the Brillouin threshold, steady state is assumed for all the waves. If the Raman pump is assumed undepleted Eqs. (1a) and (2a) give

$$P_R^+(z) = \tilde{P}_R^+ \exp(-\alpha_R z), \tag{14a}$$

$$P_R^-(z) = \tilde{P}_R^- \exp\left[-\alpha_R(L-z)\right], \tag{14b}$$

with the effective Raman input powers and attenuated reflectivities defined as

$$\tilde{P}_R^\pm = \frac{P_R^{\mathrm{in},\pm} + \tilde{R}_R^\pm P_R^{\mathrm{in},\mp}}{1 - \tilde{R}_R^+ \tilde{R}_R^-}, \qquad \tilde{R}_R^\pm = R_R^\pm \exp(-\alpha_R L). \tag{15}$$

Furthermore, assuming negligible influence from the SBS on the signal, Eqs. (1b) and (2b) yield

$$P_S^+(z) = \tilde{P}_S G^+(z), \tag{16a}$$

$$P_S^-(z) = \rho_- \tilde{P}_S G^+(L) G^-(z), \tag{16b}$$

where the effective signal input power and the effective reflectivities are defined as

$$\tilde{P}_S = \frac{P_S^{\mathrm{in}}}{1 - \rho_S^+ \rho_S^-}, \qquad \rho_i^\pm = R_i^\pm G^+(L), \tag{17}$$

and the effective Raman gain as

$$G^\pm(z) = \exp\left\{ \mp \alpha z \pm \frac{g_R}{\alpha_R} \left[\tilde{P}_R^+ \left(1 - e^{-\alpha_R z}\right) + \tilde{P}_R^- e^{-\alpha_R L} \left(e^{\alpha_R z} - 1\right) \right] \right\}. \tag{18}$$

Using Eqs. (1c) and (2c) the Brillouin wave is then given by

$$P_B^+(z) = \tilde{P}_B^+ G^+(z) \exp\left[g_B \tilde{P}_S \rho_- J^+(z)\right], \tag{19a}$$

$$P_B^-(z) = \tilde{P}_B^- G^-(z) \exp\left[g_B \tilde{P}_S J^-(L)\right] \exp\left[-g_B \tilde{P}_S J^-(z)\right], \tag{19b}$$

where the effective Brillouin input powers and the effective Brillouin positions are defined as

$$\tilde{P}_B^\pm = \frac{\varepsilon^\pm + \tilde{\rho}_B^\pm \varepsilon^\mp}{1 - \tilde{\rho}_B^+ \tilde{\rho}_B^-}, \qquad J^+(z) = G^+(L) \int_0^z G^-(z')\mathrm{d}z', \qquad J^-(z) = \int_0^z G^+(z')\mathrm{d}z', \tag{20}$$

and the effective Brillouin reflectivities as

$$\tilde{\rho}_B^- = \rho_B^- \exp\left[+g_B \tilde{P}_S \rho_S^- J^+(L)\right], \qquad \tilde{\rho}_B^+ = \rho_B^+ \exp\left[-g_B \tilde{P}_S J^-(L)\right]. \tag{21}$$

Appendix B.

The evolution integrals $J_S^\pm(z)$, Eqs. (8), can be written on the form

$$J_S^\pm(z) = \int_0^z a_\pm \exp\left[\alpha_\pm z' - b_\pm \exp(\alpha_\pm z') + c_\pm \exp(-\alpha_\pm z')\right] dz', \qquad (22)$$

where the coefficients $a_\pm$, $\alpha_\pm$, $b_\pm$ and $c_\pm$ can be found by comparison to Eqs. (8).

Introducing the change of variables $x = \exp(\alpha_\pm z)$, $1/\alpha_\pm dx = \exp(\alpha_\pm z)dz$ gives

$$
\begin{aligned}
J_S^\pm(x) &= \frac{a_\pm}{\alpha_\pm} \int_{x(0)}^{x(z)} \exp(-b_\pm x' + c_\pm x'^{-1}) dx' \\
&= \frac{a_\pm}{\alpha_\pm} \int_{x(0)}^{x(z)} \exp\left\{ -\frac{2\sqrt{b_\pm c_\pm}}{2} \left[\sqrt{\frac{b_\pm}{c_\pm}}x' - \left(\sqrt{\frac{b_\pm}{c_\pm}}x'\right)^{-1} \right] \right\} dx' \\
&= \frac{a_\pm}{\alpha_\pm} \int_{x(0)}^{x(z)} \sum_{n=-\infty}^{\infty} J_n(2\sqrt{b_\pm c_\pm}) \left(-\sqrt{\frac{b_\pm}{c_\pm}}x'\right)^n dx',
\end{aligned}
\qquad (23)
$$

where in the last line the generating function for the Bessel function of the first kind, $J_n(x)$ has been used. The integral yield

$$J_S^\pm(x) = \frac{a_\pm}{\alpha_\pm} \sum_{\substack{n=-\infty \\ n \neq -1}}^{\infty} \frac{J_n(2\sqrt{b_\pm c_\pm})}{n+1} \left(-\sqrt{\frac{b_\pm}{c_\pm}}\right)^n (x^{n+1} - 1) + \frac{a_\pm}{\alpha_\pm}\sqrt{\frac{c_\pm}{b_\pm}}J_1(2\sqrt{b_\pm c_\pm})\ln(x). \quad (24)$$

In the current work numerical integration has been used to solve $J^\pm(L)$ in solving the implicit Eqs. (10) and (11).